

MIT Open Access Articles

Simulation of Fluid-Structure Interaction in Extracorporeal Membrane Oxygenation Circulatory Support Systems

The MIT Faculty has made this article openly available. **Please share** how this access benefits you. Your story matters.

Citation: Nezami, Farhad R., Ramezanpour, Mehdi, Khodaei, Farhan, Goffer, Efrat, Edelman, Elazer R. et al. 2021. "Simulation of Fluid-Structure Interaction in Extracorporeal Membrane Oxygenation Circulatory Support Systems."

As Published: <https://doi.org/10.1007/s12265-021-10143-7>

Publisher: Springer US

Persistent URL: <https://hdl.handle.net/1721.1/141707>

Version: Author's final manuscript: final author's manuscript post peer review, without publisher's formatting or copy editing

Terms of use: Creative Commons Attribution-Noncommercial-Share Alike



Simulation of Fluid-Structure Interaction in Extracorporeal Membrane Oxygenation Circulatory Support Systems

Cite this article as: Authors: Farhad R. Nezami, PhD, Mehdi Ramezani, PhD, Farhan Khodaei, Efrat Goffer, Elazer R. Edelman, MD, PhD, Steven P. Keller, MD, PhD, Simulation of Fluid-Structure Interaction in Extracorporeal Membrane Oxygenation Circulatory Support Systems, *Journal of Cardiovascular Translational Research*, doi: [10.1007/s12265-021-10143-7](https://doi.org/10.1007/s12265-021-10143-7)

This Author Accepted Manuscript is a PDF file of an unedited peer-reviewed manuscript that has been accepted for publication but has not been copyedited or corrected. The official version of record that is published in the journal is kept up to date and so may therefore differ from this version.

Terms of use and reuse: academic research for non-commercial purposes, see here for full terms. <http://www.springer.com/gb/open-access/authors-rights/aam-terms-v1>

Author accepted manuscript

Simulation of Fluid-Structure Interaction in Extracorporeal Membrane Oxygenation Circulatory Support Systems

Authors: Farhad R. Nezami, PhD^{1,2}, Mehdi Ramezanpour³, Farhan Khodaei¹, Efrat Goffer¹, Elazer R. Edelman, MD, PhD^{1,4}, Steven P. Keller, MD, PhD^{1,5}

Institutions:

¹Institute for Medical Engineering and Science, Massachusetts Institute of Technology, Cambridge, MA, USA

²Department of Surgery (Thoracic and Cardiac Surgery), Brigham and Women's Hospital, Harvard Medical School, Boston, MA, USA

³Department of Mechanical Engineering, University of Pittsburgh, Pittsburgh, PA, USA

⁴Department of Medicine (Cardiovascular Medicine), Brigham and Women's Hospital, Harvard Medical School, Boston, MA, USA

⁵Department of Medicine (Pulmonary and Critical Care Medicine), Brigham and Women's Hospital, Harvard Medical School, Boston, MA, USA

Corresponding author:

Dr. Steven P. Keller

Division of Pulmonary and Critical Care Medicine

Brigham and Women's Hospital

75 Francis Street Boston, MA, USA 02115

Email: spkeller@mit.edu

Word count: 3390

Author accepted manuscript

Abbreviations:

Fr	French (unit of measurement)
kg	kilogram
m	meter
L	liter
LPM	liter per minute
ECMO	extracorporeal membrane oxygenation
CFD	computational fluid dynamics
MCS	mechanical circulatory support
VOF	Volume of Fluid
Q	flow
C	capacitance
R	resistance
BCA	brachiocephalic artery
LCCA	left common carotid artery
LSA	left subclavian artery
CA	celiac artery
SMA	superior mesenteric artery
LRA	left renal artery
RRA	right renal artery
IMA	inferior mesenteric artery
LCI	left common iliac artery
RCI	right common iliac artery

ABSTRACT

Extracorporeal membrane oxygenation (ECMO) is a vital mechanical circulatory support modality capable of restoring perfusion for the patient in circulatory failure. Despite increasing adoption of ECMO there is incomplete understanding of its effects on systemic hemodynamics and how the vasculature responds to varying levels of continuous retrograde perfusion. To gain further insight into the complex ECMO:failing-heart circulation, computational fluid dynamics simulations focused on perfusion distribution and hemodynamic flow patterns were conducted using a patient-derived aorta geometry. Three case scenarios were simulated: (1) healthy control; (2) 90% ECMO-derived perfusion to model profound heart failure; and, (3) 50% ECMO-derived perfusion to model the recovering heart. Fluid-structure interface simulations were performed to quantify systemic pressure and vascular deformation throughout the aorta over the cardiac cycle. ECMO support alters pressure distribution while decreasing shear stress. Insights derived from computational modeling may lead to better understanding of ECMO support and improved patient outcomes.

Key words: extracorporeal membrane oxygenation, mechanical circulatory support, fluid-structure interaction, computational fluid dynamics

INTRODUCTION

Extracorporeal membrane oxygenation (ECMO) is increasingly deployed to provide mechanical circulatory support (MCS) for cardiogenic shock patients¹⁻⁴. Despite growing use, overall mortality for shock patients supported by ECMO remains near 50% and is comparable to survival rates for medical therapy alone⁵⁻⁸. Morbid complications and poor outcomes abound even with titration of support to traditional hemodynamic metrics⁹⁻¹³. These limitations highlight the need for greater understanding of complex device-patient interactions to monitor and modulate support to optimize clinical outcomes.

ECMO provides circulatory support by shunting venous blood through a gas exchange device to return oxygenated blood to the systemic circulation¹⁴. In its most commonly implemented form in the adult patient with circulatory failure, venous blood is withdrawn via a multistage cannula inserted through the femoral vein and advanced to the level of the caval-atrial junction. The ECMO circuit then returns oxygenated blood through a cannula inserted into the femoral artery which terminates in the iliac artery or distal aorta depending on patient anatomy¹⁴⁻¹⁶.

In this cannulation approach, ECMO provides continuous retrograde perfusion into the distal aorta which then collides with pulsatile antegrade perfusion from the heart to create a dynamic watershed region with mixing of the colliding flows^{17,18}. The complex hybrid circulation generated by dual perfusion from the ECMO circuit and the heart, termed here as the ECMO:failing heart circulation¹⁸, differs significantly from physiologic ventriculo-vascular interactions as the left ventricle ejects against

continuous retrograde filling of the aorta. The effects of this new circulation on the vasculature and vascular response are not fully delineated.

In vivo assessment of these elements is limited by challenges in determining and controlling experimental inputs and measuring and quantifying observed metrics to yield meaningful results. Computational models provide strict control of input variables to yield insight into the multitude of competing and intertwined factors that determine patient-device interactions and enable precise study of the effects of ECMO support on systemic hemodynamics^{19,20}. Prior work quantified flow distribution in the ECMO-failing heart circulation using an idealized geometry of the aortofemoral vasculature and analyzed watershed region dynamics over the cardiac cycle¹⁸. The current study investigates the complex interactions between the combined flow generated by the heart and the ECMO circuit and the vasculature using a subject-specific aortic geometry adapted from clinical imaging. Further insight into the effects of ECMO support on perfusion and the vascular response may lead to new metrics to guide the use of support and improved clinical outcomes.

METHODS

Anatomical Geometry

A subject-specific vascular geometry was reconstructed from de-identified clinical computer tomography angiography (CTA) images in accordance with an approved local IRB protocol (Figure 1). DICOM images were segmented semi-automatically using the open source ITK-snap package²¹. The reconstructed model consisted of the aorta starting from the sinotubular junction and extending distally through the iliac bifurcation. The main aortic branches were also reconstructed and included the brachiocephalic artery (BCA), left common carotid artery (LCCA), left subclavian artery (LSA), celiac artery (CA), superior mesenteric artery (SMA), left and right renal arteries (LRA and RRA), inferior mesenteric artery (IMA), and left and right common iliac arteries (LCI and RCI). The resulting point-cloud geometry was exported as STL, and further refined and smoothed using MeshLab²². A 15-French cannula was numerically added to the system in the process of grid generation to model source of ECMO-supplied perfusion. The cannulation site modeled as the left femoral vein at a location comparable to standard clinical practice.

Grid Generation

Following the previously described grid generation procedure^{18,23}, the fluid domain was discretized using tetrahedral elements using ANSYS Meshing (ANSYS v. 17.2, Canonsburg, PA, USA). The thickness of near wall elements was set to ensure Y^+ values were within the desirable range. The initial computation domain was uniformly and sequentially refined until grid-independent results were attained. Element

sizing at areas with relatively lower gradient of flow velocity was refined the least to reduce computational burden.

Computational Method

The governing equations and numerical methods used in this study have been previously described in detail²⁴. The transient three-dimensional turbulent multiphase flow of blood and ECMO fluid was modeled using compliant walls. The homogeneous multiphase model as a sub-branch of Eulerian-Eulerian multiphase flow was considered to attain the velocity field. Appropriate interface transfer model was applied to simulate the interactions between the two phases¹⁸. This model enables capturing the watershed region, which is defined as the interface created by the collision of the heart and ECMO blood. The blood is modeled as a homogeneous, incompressible and Newtonian fluid with the dynamic viscosity of 0.0035 Pa S and the density of 1060 kg/m³. The initial conditions of the simulations for the velocity vector components and pressure were set to zero, but the simulations were performed adequately long, multiple cardiac cycles, to achieve a periodic repeatable flow behavior. For transient FSI simulations, the initial conditions are of high importance in achieving the desirable convergence behavior. Herein, steady state FSI simulations were used to initialize the transient FSI simulations. The detailed procedure of this initialization step is previously described²³. The flow regime at the vicinity of the cannula outlets was considered turbulent with the resultant flow approximated using the shear stress transport (SST) model.

Boundary Conditions

Blood enters the computational domain as antegrade flow from the left ventricular outlet and as retrograde flow from the ECMO cannula. An area-averaged, subject-

specific velocity profile was used to define a three-dimensional parabolic velocity profile that was then applied at the entrance of ascending aorta²⁵. To define this parabolic profile, the hydraulic diameter of the entrance of the ascending aorta was extended from the inlet of the computational domain sufficiently enough to eliminate spatiotemporal effects arising from differences between the entrance cross-section and a perfectly circular shape. To model a patient stably supported on ECMO with varying degrees of heart failure, steady-state flow of oxygenated blood was applied at the inlet of the cannula such that the combination of both inlets added up to a total flow rate of 5 LPM to approximate total systemic perfusion in a typical adult at rest. To investigate the variability of interactions between the compliant vascular wall and complex flow elements and how it is changes with heart recovery and decreasing ECMO support, two different ECMO-assisted cases were modeled and compared to the healthy state. The ECMO-assisted cases were distinguished by the relative percent of total perfusion provided by the ECMO-circuit. To model profound heart failure, ECMO flow consisting of 90% of total perfusion was applied while the recovering heart case was modeled with ECMO providing 50% of the total perfusion. These two flow distributions were selected as bounds of the clinical trajectory of the stably supported patient progressing from profound failure to recovery.

A three-element lumped parameter model was applied at the domain exits to provide dynamic boundary conditions as previously described^{18,26}. The equation to be iteratively solved to relate the pressure and flowrate at the aortic tree outlets is given as:

$$\frac{\partial p}{\partial t} + \frac{p}{CR_d} = \frac{Q}{C} \left(1 + \frac{R_p}{R_d} \right) + R_p \frac{\partial Q}{\partial t}$$

where P and Q are the pressure and flow rate at individual aortic exits, C is the compliance, and R_p and R_d are the proximal and distal vasculature resistances, respectively.

Simulations were performed on a high-performance computer cluster using distributed parallel processing nodes. Blood velocity fields and mesh elements displacements were extracted from computation results for further analysis.

Author accepted manuscript

RESULTS

Blood flow and structural mechanics of the vasculature were simulated in a patient-specific model to study blood flow and its interaction with a distensible aorta. The circulation of the vasculature and structural responses were analyzed in the healthy case and the ECMO-failing heart system at two differing levels of heart function: (1) relative ECMO flow of 90% of total perfusion to model support during profound heart failure and (2) relative ECMO flow of 50% to model support during cardiac recovery.

The local, time-varying hemodynamic effects of the retrograde ECMO jet on global patterns of the flow were quantified (Figure 2). Blood flow streamlines in the healthy case demonstrate symmetric perfusion of peripheral arteries with accelerated flow near aortic exits as luminal diameters tapered. The anterior-posterior distribution of aortic flow coupled with inherent inertia generates a helical flow pattern at the aortic arch that is streamlined and laminar. Introduction of the aberrant, high-speed jet of the ECMO return cannula induces asymmetry in hemodynamics of distal arteries, imposing retrograde forces that oppose the antegrade stream of the heart. In the face of 50% ECMO support this disturbance mainly affects the abdominal and distal regions. When ECMO return is dominant and accounts for 90% of the flow the vertical disturbances and complex chaotic structures extend proximally up the aorta to the aortic arch and the outlets of the great vessels.

To further analyze the effect of ECMO support on hemodynamic patterns in distensible vessels, the time-varying pressure was quantified throughout the vasculature. Each case was initialized to an identical reference pressure but then varied significantly over the cardiac cycle as a result of different resistances in front of the

systemic circulation and varying pulsatility of flow structures (Figure 3). In the healthy case, pressure at the arterial wall increases with ejection of blood from the ventricle during systole and then decreases with blood deceleration and closure of the aortic valve. Blood flow pulsatility produced by cardiac contraction results in temporal variability in the arterial wall pressure observed over the cardiac cycle. Introduction of ECMO support upregulates the pressure in the system for the entirety of the cardiac cycle due to the resistance of two competing antegrade and retrograde flow streams in the system. The temporal variability of the pressure is decreased with increasing relative flow provided by ECMO as the pulsatile component from cardiac contraction is decreased.

As observed in the pressure distribution, the watershed region created by the collision of continuous retrograde flow from the ECMO circuit and pulsatile antegrade flow generated by the heart plays a crucial role in determining the hemodynamic profile. The watershed region was quantified through determining the volume fractions of the mixed blood overlaid on the flow streamlines (Figure 4). The result confirms the confinement of the watershed region to the abdomen in the 50% ECMO case and the aortic arch (proximal outlets) in the 90% ECMO flow case. Dynamics of the mixing zone are governed by the interplay of antegrade and retrograde flow over the cardiac cycle.

Wall shear stress (WSS) was quantified throughout the aortic geometry over the cardiac cycle for each case (Figure 5). Time-averaged WSS demonstrated a significant peak at the vicinity of the cannulation site in the ECMO cases with the maximum observed for the 90% ECMO case consistent with the shear forces exerted by the high-speed jet from the cannula. The asymmetric pattern of flow and pressure at peripherals

during ECMO support was again detected compared to the healthy heart case. Location of the watershed region determined the distribution of the WSS at the proximal aorta and abdomen for cases with ECMO support.

Modeling the interaction of blood and the vasculature enables quantification of different structural response components, including the principal stress and strain at the wall and the total vascular deformation. We first present the principal stress in three studied cases, adding an insert of the stress map from the posterior view to complement the analysis (Figure 6). Higher maximum principal stress in healthy case was observed and concentrated in the proximal aorta in comparison with the ECMO support cases. The pattern of stress follows the observed flow patterns. As a result of elastic behavior of the aorta, the strain map also follows a similar pattern to the principal stress (Figure 7). In proximal regions, strain follows similar patterns as a result of observed stress distribution. Cannulation of the femoral artery was observed not to significantly enlarge or deform the femoral and iliac arteries. The contour of strain shows the 50% ECMO case bearing slightly more strain than the 90% case despite increased jet from the ECMO cannula with increased flow. The deformation map displays a similar distribution at the proximal aorta but differs in the iliac and femoral arteries as ECMO flow increases (Figure 8). The combined effects of higher pressure and the cannula's jet flow inertia cause more deformation on the LCI for the 90% case compared to that of the 50% (Video 1 in Supplementary Materials) further explained in the discussion section.

DISCUSSION

ECMO is capable of rapidly restoring systemic perfusion for patients in profound shock¹⁴. Yet, despite increasing adoption, its hemodynamic consequences remain challenging to define and optimize. In absence of mechanistic insight into the effects of ECMO support on cardiac and vascular state, practitioners rely largely on guidelines drawn from clinical experience and expert consensus to determine patient care and device management. There is urgent need to advance understanding of the complex ECMO: failing heart circulation to harness the therapeutic potential of this support modality and improve patient outcomes.

The ECMO: failing heart circulation is a profound departure from the intact physiological circulation in health²⁷. Retrograde perfusion from the ECMO return cannula alters normal blood flow and may affect both perfusion and cardiac load. The watershed region established by collision of antegrade flow from the failing heart with retrograde perfusion from the ECMO circuit is a dynamic mixing region that moves within the aorta over the cardiac cycle whose size and position is a function of relative ECMO flow and vascular anatomy¹⁸. Simultaneously, increased afterload from retrograde perfusion may act to decrease ejection from the left ventricle and decrease cardiac efficiency.

These effects become more prominent as ECMO flow relative to native flow increases. The pressure wave generated by the left ventricle and its propagation into the vascular tree in health is a complex interplay between volume of blood ejected, contractile force of the heart, and compliance of the vasculature and left ventricle^{28–32}. ECMO reduces peak velocity throughout the cardiac cycle (Figure 2) and the extent of

the distal propagation of the pressure impulse (Figure 3). As the fraction of total perfusion is shifted from the heart and to the ECMO circuit, peak pressure in the aorta decreases with decreasing magnitude of the cardiac impulse. This leads to progressively smaller variations in aortic pressure over the cardiac cycle as ECMO support increases.

Normal blood flow in the aorta in health is highly pulsatile and varies over the cardiac cycle (Figure 3). In comparison, ECMO circulatory support reduces the magnitude of the ventricular pulse wave by shunting blood away from the heart to thereby reduce peak systolic pressure and increase diastolic pressure. ECMO flow increases more spatial variability to the pressure distribution in comparison to the healthy condition as a result of resistance introduced by retrograde flow but is less temporally variable due to the decreased pulsatility. As ECMO support increases, pressure distribution is more uniform both spatially and temporally over the cardiac cycle.

The location of the watershed region within the aorta is determined by the relative fraction of flow provided by the ECMO circuit (Figure 4). As flow through the circuit increases relative to the flow generated by the heart, the watershed region is pushed proximally in the aorta. The site of the watershed region may have important clinical ramifications as the turbulent flow within the region may be a source of decreased perfusion to branching vessels or may lead to areas of stasis at risk for clot formation and potential embolic injury to end organs. The watershed region also determines the transition zone in the aorta where the source of end-organ perfusion changes from the heart to the ECMO circuit. This site is of particular concern in the

setting of concomitant lung disease and the potential for differential oxygenation of tissues.

A further source of potential injury is alteration in wall shear stress experienced by the specific regions of the vascular tree during ECMO support (Figure 5). In the healthy case, wall shear stress is experienced proximally within the aorta and then at sites of branching vessels as the impulse wave advances antegrade following left ventricular contraction. In the setting of 90% ECMO flow, the proximal shear stress is greatly reduced as the antegrade impulse wave is much smaller in magnitude while greater stress is present at the site of ECMO cannulation and delivery of high velocity retrograde flow. The potential for thromboembolism from disruption of wall plaques in the femoral and iliac vessels is an important clinical consideration in the setting of high levels of ECMO support. The case of 50% ECMO flow represented a relative trough between the two extremes as both peak ECMO flow and cardiac impulse magnitude were reduced resulting in lower wall shear stress than either extreme situation.

The shunting of blood to the arterial system and the generation of retrograde perfusion of the aortic tree by the ECMO circuit represents a profound departure from intact ventriculo-vascular coupling in health^{27,33}. In the healthy scenario, ventriculo-vascular coupling is determined by the elastance of the vasculature and the ventricle. ECMO alters this relationship by maintaining continuous retrograde perfusion of the aorta throughout the cardiac cycle. The pattern of physical deformation of the aorta over the cardiac cycle varies substantially from the healthy case to ECMO-supported cases (Figure 8).

This study seeks to quantify both vascular deformation and stress. Deformation in the healthy artery predominantly occurs at the distal aorta and peripheral vessels as pulsatile flow reaches the smaller diameters distal vessels. The flow structure in those areas induce the translational deformation (Figure 8). The strain observed is the immediate result of pressure distribution with more pronounced strain occurring at areas experiencing higher pressure and stress (Figure 7). Strain during ECMO support results from interaction of the high velocity ECMO jet and pulsatile heart flow. The interaction of pulsatile native heart flow and retrograde ECMO flow generates a complex hemodynamic structure that modulates pressure distribution and flow patterns (Figure 3). In the 50% ECMO case, resistance induced by retrograde perfusion and the impulse from antegrade flow elevate pressure on the vascular wall and produce higher strain than the 90% ECMO case due to the relative decrease in cardiac impulse (Figure 7).

The largest degree of stress observed in the healthy case occurs in the proximal aorta when the entire systemic perfusion is provided by the heart. Contrasting this scenario with the 90% ECMO case, in which systemic perfusion mostly consists of continuous retrograde flow from the ECMO circuit provided over the duration of the cardiac cycle, vascular deformation and strain are markedly reduced. The combined effect of ECMO support is to decouple the ventricle and vasculature and alter the vascular state. These induced changes may be potential avenues of investigation to determine new metrics to guide titration of ECMO support and to further inform overall management of the shock patient.

LIMITATIONS AND FUTURE WORK

The goal of the present study is to advance understanding of the interaction of hemodynamics and mechanics in the ECMO-failing heart circulation system. FSI simulation, in addition to resolving aberrant flow patterns, is capable of estimating mechanical forces and deformation in the vasculature. Further insight may lead to modification of ECMO support titrated to a patient's specific response with a more informed selection of working parameters, enhanced risk stratification, and improved clinical decision making.

Although numerical methods provide a robust tool to explore mechanical circulatory support systems, there are limitations with this approach. Variable flow from the ECMO circuit modulates both cardiac afterload and preload and may also alter physiological vascular responses which will significantly change systemic hemodynamics and affect end-organ perfusion. The range of physiological interactions and the complex interplay between ECMO circuit and the heart are challenging to model and are deferred to future studies to permit focus of the current work on the hemodynamics of hybrid flows. In addition, more diverse selection of patient-specific cases with parameter/sensitivity studies on different components of the numerical model are required to reduce the bias and achieve generalizable conclusions. The computational cost of intensive FSI simulation limits the feasible range of parameters for study. A final consideration is that the boundary conditions applied in this work are general and based on average values of resistance and compliance for healthy subjects. Patient-specific boundary condition setting would allow more realistic outcomes while FSI would enable the dynamic study of the vascular response to

cardiogenic shock and the subsequent initiation of mechanical circulatory support. Future work will address these challenges in an effort to expand understanding of ECMO and its interaction with the cardiovascular system.

Author accepted manuscript

COMPLIANCE WITH ETHICAL STANDARDS

Disclosures

E.R.E. reports receiving a research grant from Abiomed, Inc. S.P.K. reports serving on the Abiomed, Inc. Critical Care Advisory Board. E.R.E. and S.P.K. are co-inventors on submitted patent applications on subjects broadly relevant to mechanical circulatory support. The authors deny any other disclosures relevant to the submitted work.

Human subjects

No human studies were carried out by the authors for this article. De-identified patient imaging data was used for this article in accordance with Institutional Review Board approval.

Informed consent

Institutional Review Board provided a waiver for obtaining informed patient consent.

Animal studies

No animal studies were carried out by the authors for this article.

Sources of Funding:

SPK supported by NHLBI 5K08HL14332

ERE supported by NIH R0149039

REFERENCES

1. Lorusso R, Alexander P, Rycus P, Barbaro R. The Extracorporeal Life Support Organization Registry: update and perspectives. *Ann Cardiothorac Surg*. 2019;8(1):93-98. doi:10.21037/acs.2018.11.03
2. Paden ML, Conrad SA, Rycus PT, Thiagarajan RR, ELSO Registry. Extracorporeal Life Support Organization Registry Report 2012. *ASAIO J*. 2013;59(3):202-210. doi:10.1097/MAT.0b013e3182904a52
3. Ghodsizad A, Koerner MM, Brehm CE, El-Banayosy A. The role of extracorporeal membrane oxygenation circulatory support in the “crash and burn” patient: From implantation to weaning. *Curr Opin Cardiol*. 2014;29(3):275-280. doi:10.1097/HCO.0000000000000061
4. Khan MH, Corbett BJ, Hollenberg SM. Mechanical circulatory support in acute cardiogenic shock. *F1000Prime Rep*. 2014;6(3):91. doi:10.12703/P6-91
5. Goldberg RJ, Samad NA, Yarzebski J, Gurwitz J, Bigelow C, Gore JM. Temporal trends in cardiogenic shock complicating acute myocardial infarction. *N Engl J Med*. 1999;340(15):1162-1168.
6. Reyentovich A, Barghash MH, Hochman JS. Management of refractory cardiogenic shock. *Nat Rev Cardiol*. 2016;13(8):481-492. doi:10.1038/nrcardio.2016.96
7. Karagiannidis C, Brodie D, Strassmann S, et al. Extracorporeal membrane oxygenation: evolving epidemiology and mortality. *Intensive Care Med*. 2016;42(5). doi:10.1007/s00134-016-4273-z
8. El Sibai R, Bachir R, El Sayed M. ECMO use and mortality in adult patients with

- cardiogenic shock: a retrospective observational study in U.S. hospitals. *BMC Emerg Med.* 2018;18(1):20. doi:10.1186/s12873-018-0171-8
9. Ventetuolo CE, Muratore CS. Extracorporeal Life Support in Critically Ill Adults. *Am J Respir Crit Care Med.* 2014;190(5):497-508. doi:10.1164/rccm.201404-0736CI
 10. Aubron C, Cheng AC, Pilcher D, et al. Factors associated with outcomes of patients on extracorporeal membrane oxygenation support: a 5-year cohort study. *Crit Care.* 2013;17(2):R73. doi:10.1186/cc12681
 11. Bisdas T, Beutel G, Warnecke G, et al. Vascular Complications in Patients Undergoing Femoral Cannulation for Extracorporeal Membrane Oxygenation Support. *Ann Thorac Surg.* 2011;92(2):626-631. doi:10.1016/J.ATHORACSUR.2011.02.018
 12. Cheng R, Hachamovitch R, Kittleson M, et al. Complications of extracorporeal membrane oxygenation for treatment of cardiogenic shock and cardiac arrest: A meta-analysis of 1,866 adult patients. *Ann Thorac Surg.* 2014;97(2). doi:10.1016/j.athoracsur.2013.09.008
 13. Abrams DC, Prager K, Blinderman CD, Burkart KM, Brodie D. Ethical dilemmas encountered with the use of extracorporeal membrane oxygenation in adults. *Chest.* 2014;145(4):876-882. doi:10.1378/chest.13-1138
 14. Keller SP. Management of Peripheral Venoarterial Extracorporeal Membrane Oxygenation in Cardiogenic Shock. *Crit Care Med.* 2019;47(9):1235-1242. doi:10.1097/CCM.0000000000003879
 15. Bartlett RH, Gattinoni L. Current status of extracorporeal life support (ECMO) for

- cardiopulmonary failure. *Minerva Anesthesiol.* 2010;76(7):534-540.
<http://www.ncbi.nlm.nih.gov/pubmed/20613694>.
16. Lequier L, Horton S, McMullan D, Bartlett RH. Extracorporeal membrane oxygenation circuitry. *Pediatr Crit care* 2013;14:1-10.
doi:10.1097/PCC.0b013e318292dd10.Extracorporeal
 17. Gehron J, Schuster M, Rindler F, et al. Watershed phenomena during extracorporeal life support and their clinical impact: a systematic in vitro investigation. *ESC Hear Fail.* 2020;7(4):1850-1861. doi:10.1002/ehf2.12751
 18. Nezami FR, Khodae F, Edelman ER, Keller SP. A Computational Fluid Dynamics Study of the Extracorporeal Membrane Oxygenation-Failing Heart Circulation. *ASAIO J.* July 2020. doi:10.1097/MAT.0000000000001221
 19. Gu K, Zhang Y, Gao B, Chang Y, Zeng Y. Hemodynamic Differences Between Central ECMO and Peripheral ECMO: A Primary CFD Study. *Med Sci Monit.* 2016;22:717-726. doi:10.12659/MSM.895831
 20. Stevens MC, Callaghan FM, Forrest P, Bannon PG, Grieve SM. A computational framework for adjusting flow during peripheral extracorporeal membrane oxygenation to reduce differential hypoxia. *J Biomech.* 2018;79:39-44.
doi:10.1016/j.jbiomech.2018.07.037
 21. Yushkevich PA, Piven J, Hazlett HC, et al. User-guided 3D active contour segmentation of anatomical structures: Significantly improved efficiency and reliability. *Neuroimage.* 2006;31(3):1116-1128.
doi:10.1016/j.neuroimage.2006.01.015
 22. Cignoni P, Callieri M, Corsini M, Dellepiane M, Ganovelli F, Ranzuglia G.

MeshLab: An Open-Source Mesh Processing Tool.

23. Ramezanpour M, Maerefat M, Ramezanpour N, Mokhtari-Dizaji M, Roshanali F, Nezami FR. NUMERICAL INVESTIGATION OF THE EFFECTS OF BED SHAPE ON THE END-TO-SIDE CABG HEMODYNAMICS. *J Mech Med Biol.* 2019;19(4). doi:10.1142/S0219519419500192
24. Ramezanpour M, Rikhtegar Nezami F, Ramezanpour N, et al. Role of Vessel Microstructure in the Longevity of End-to-Side Grafts. *J Biomech Eng.* 2020;142(2). doi:10.1115/1.4043873
25. Alastruey J, Xiao N, Fok H, Schaeffter T, Figueroa CA. On the impact of modelling assumptions in multi-scale, subject-specific models of aortic haemodynamics. *J R Soc Interface.* 2016;13(119). doi:10.1098/rsif.2016.0073
26. Rikhtegar Nezami F, Athanasiou LS, Amrute JM, Edelman ER. Vascular biology and microcirculation: Multilayer flow modulator enhances vital organ perfusion in patients with type b aortic dissection. *Am J Physiol - Hear Circ Physiol.* 2018;315(5):H1182-H1193. doi:10.1152/ajpheart.00199.2018
27. Kass DA, Kelly RP. Ventriculo-arterial coupling: concepts, assumptions, and applications. *Ann Biomed Eng.* 1992;20(1):41-62.
<http://www.ncbi.nlm.nih.gov/pubmed/1562104>. Accessed October 10, 2017.
28. Laskey WK, Parker HG, Ferrari VA, Kussmaul WG, Noordergraaf A. Estimation of total systemic arterial compliance in humans. *J Appl Physiol.* 1990;69(1):112-119.
29. Parker KH, Jones CJH, Dawson JR, Gibson DG. What stops the flow of blood from the heart? *Heart Vessels.* 1988;4(4):241-245. doi:10.1007/BF02058593
30. BAUERNSCHMITT R, MEHMANESH H, SCHULZ S, et al. Aortic Input

Impedance and Ventriculoarterial Coupling Following Cardioversion/Defibrillation.

Pacing Clin Electrophysiol. 1999;22(7):1047-1053. doi:10.1111/j.1540-

8159.1999.tb00569.x

31. Westerhof N, Lankhaar JW, Westerhof BE. The arterial windkessel. *Med Biol Eng Comput.* 2009;47(2):131-141. doi:10.1007/s11517-008-0359-2
32. Elzinga G, Westerhof N. Matching between ventricle and arterial load. An evolutionary process. *Circ Res.* 1991;68(6):1495-1500.
<http://www.ncbi.nlm.nih.gov/pubmed/2036707>. Accessed September 22, 2017.
33. Sasayama S, Asanoi H. Coupling between the heart and arterial system in heart failure. *Am J Med.* 1991;90(5B):14S-18S.
<http://www.ncbi.nlm.nih.gov/pubmed/2048567>. Accessed October 10, 2017.

FIGURES

Figure 1: Methodological steps in generating aortic geometry from clinical imaging.

Panel A: localization of vessels of interest from raw clinical images. Panel B: segmentation of aorta and major branches. Panel C: smoothing and filtering of clinical image to enable geometrical mesh formation.

Figure 2: Blood flow streamlines to visualize the hemodynamic flow patterns in the healthy and ECMO-supported cases.

Figure 3: Pressure distribution at different instances of one complete cardiac cycle in the healthy and ECMO-supported cases.

Figure 4: Watershed region shown for each ECMO-supported case as determined by the volume fraction of blood supplied by the ECMO circuit in each region (Red = 100% ECMO-supplied blood and Blue = 0% ECMO-supplied blood).

Figure 5: Time-averaged wall shear stress for the healthy and ECMO-supported cases

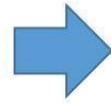
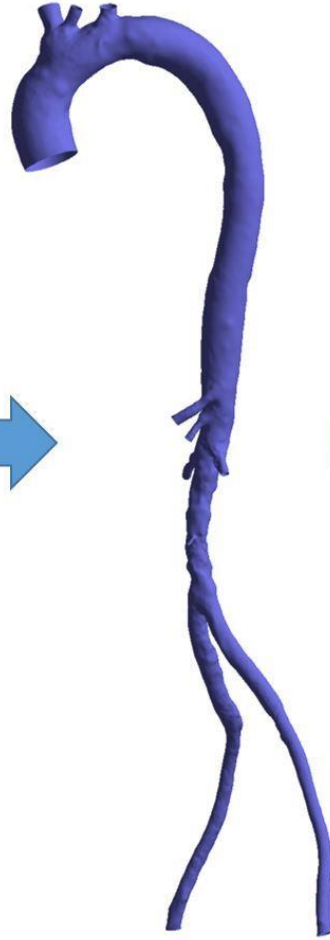
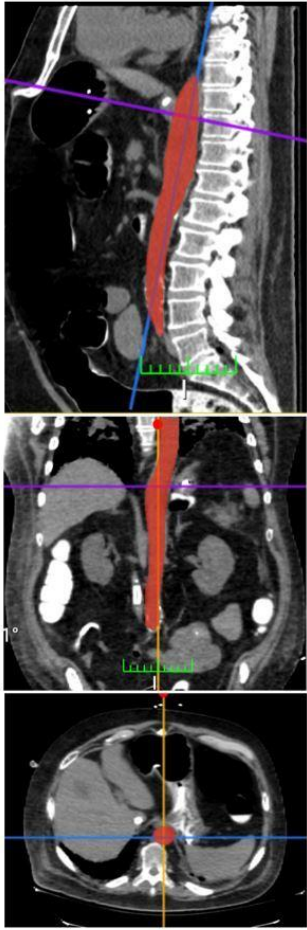
Figure 6: Maximum principal stress in the healthy and ECMO-supported cases.

Figure 7: Maximum principal strain in the healthy and ECMO-supported cases.

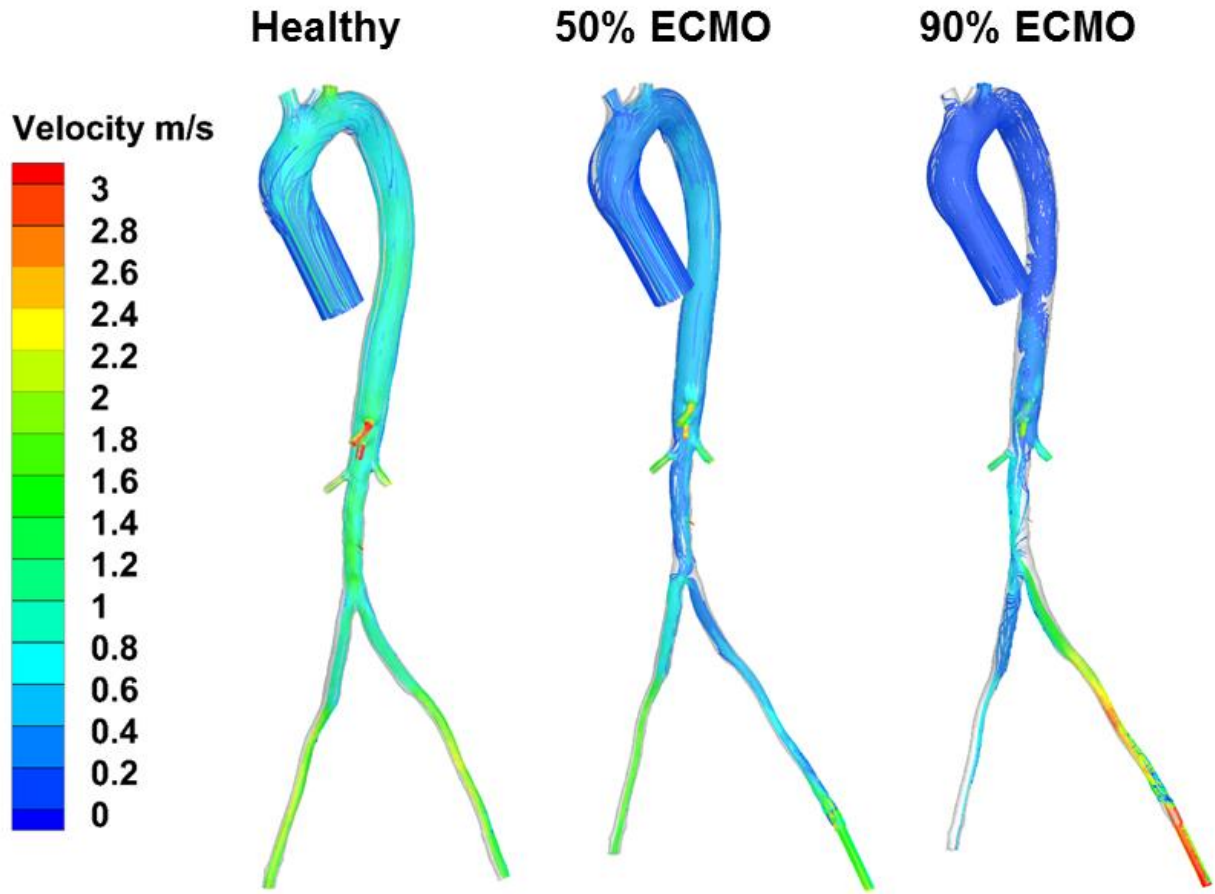
Figure 8: Maximal vascular deformation in the healthy and ECMO-supported cases.

Video Legend (available online only)

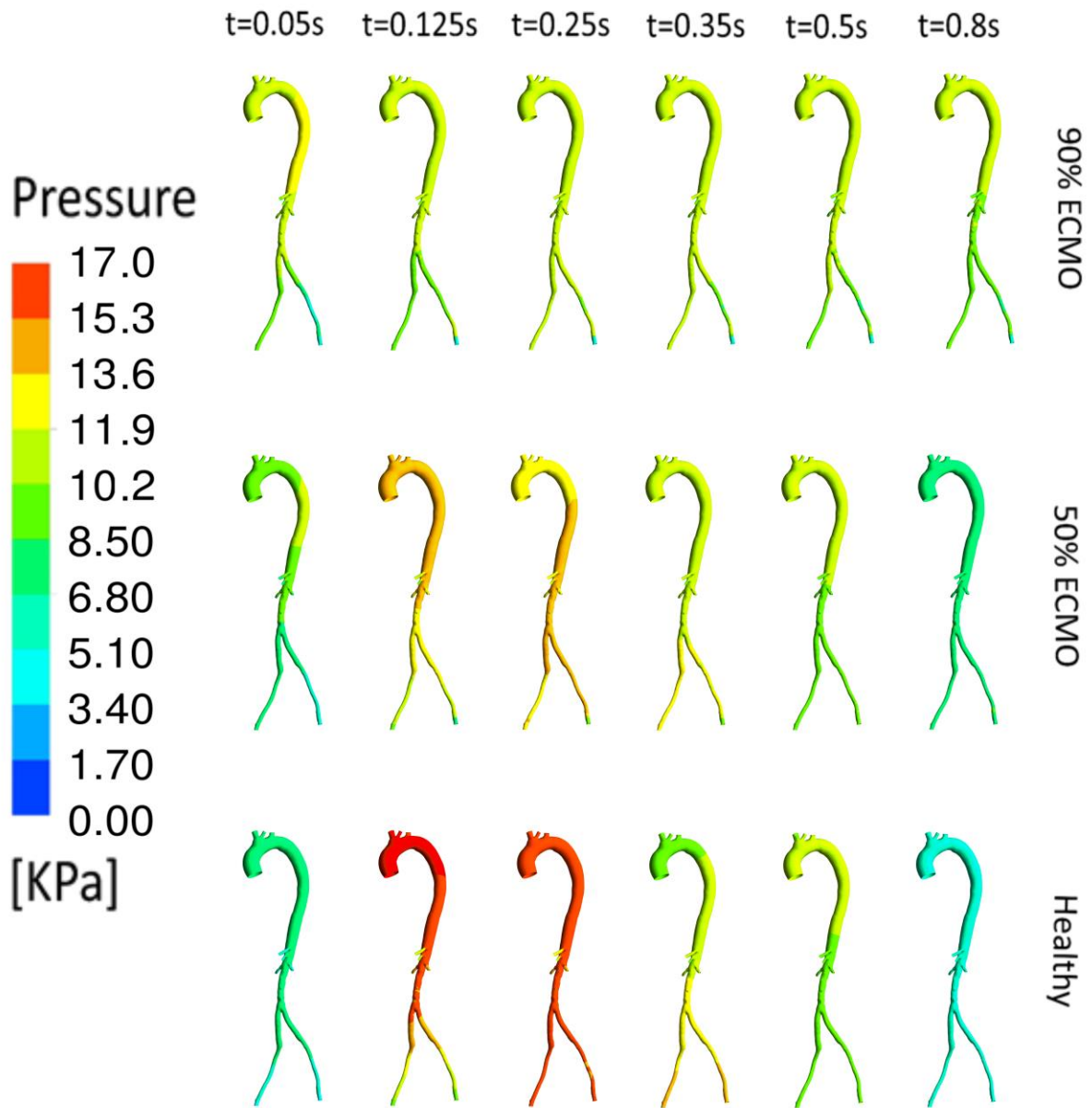
Video 1. Arterial dynamics in ECMO-failing heart circulation modeling



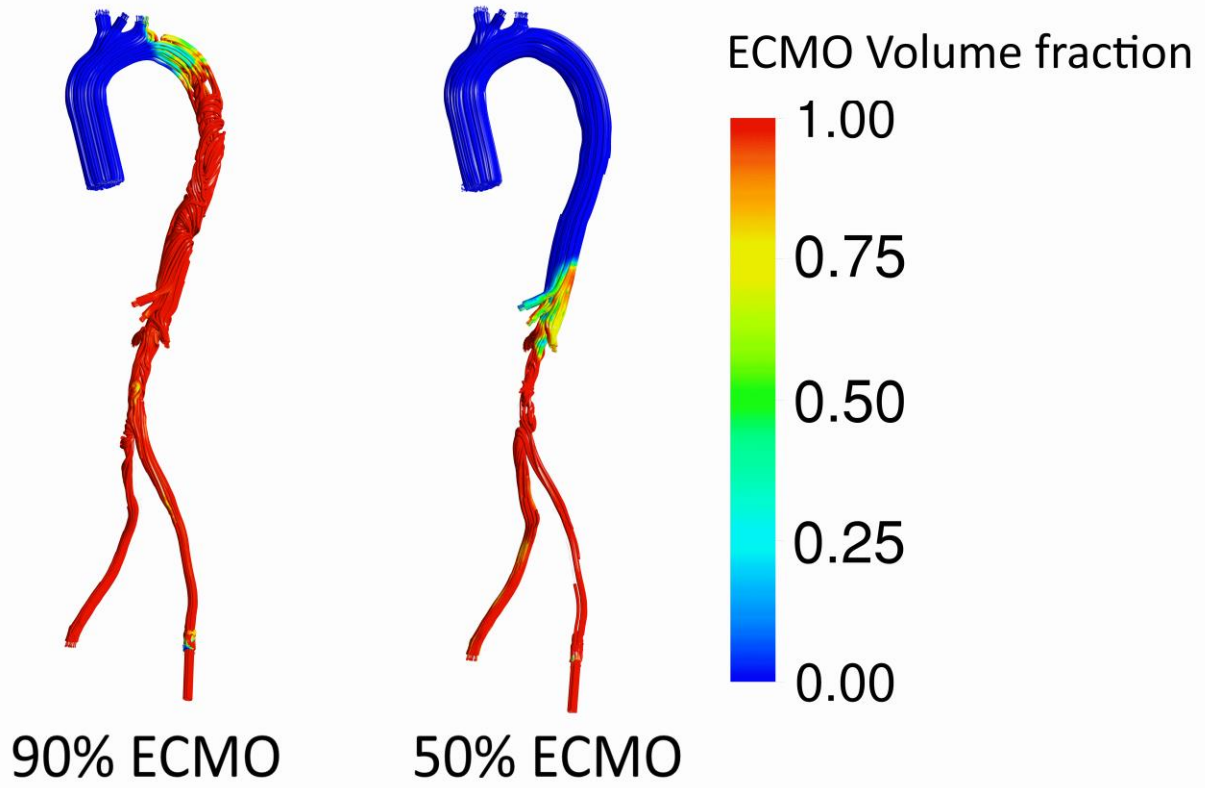
Author accepted



Author accep



AC

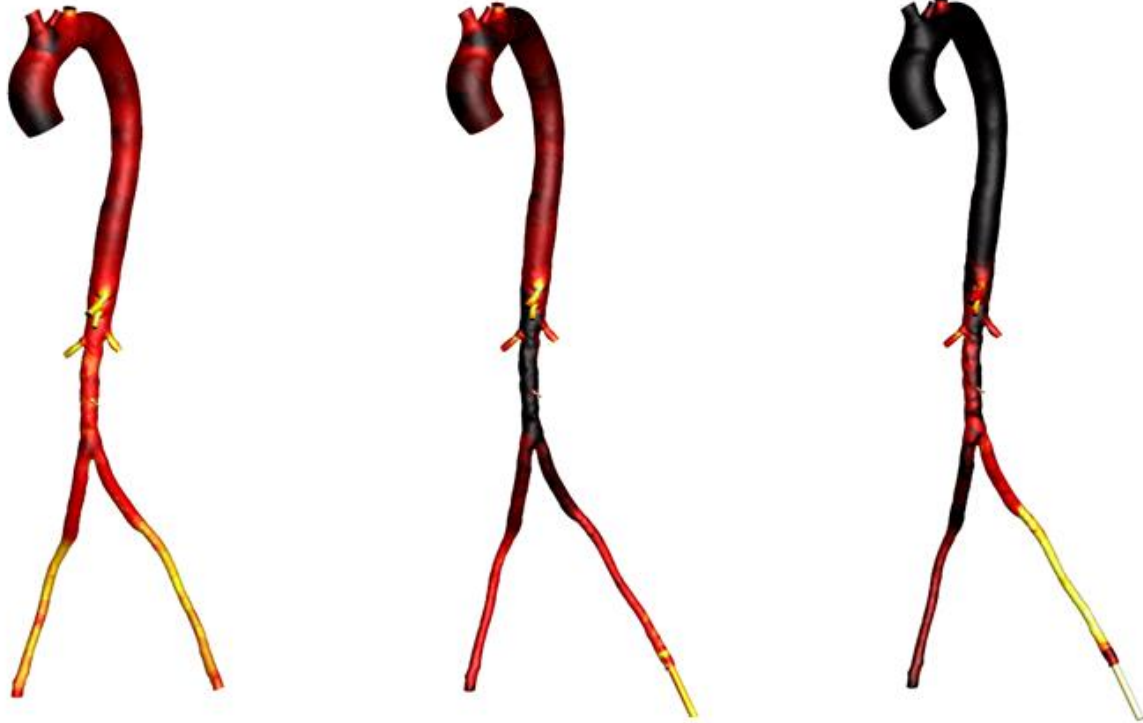


Author accepted

Healthy

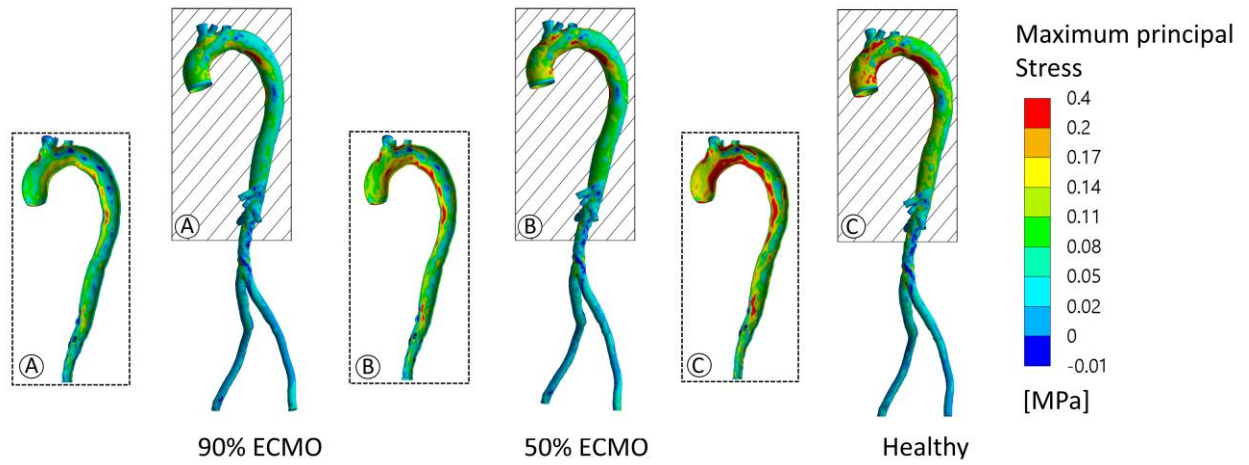
50% ECMO

90% ECMO

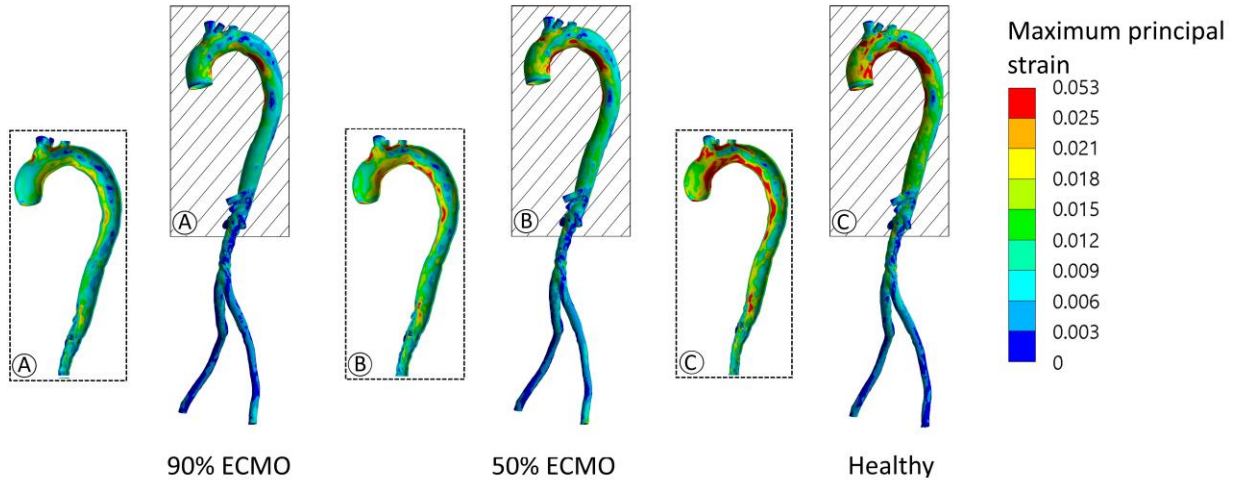


TAWSS (Pa): 1 2 3 4 6 10 16 25 40 63 100

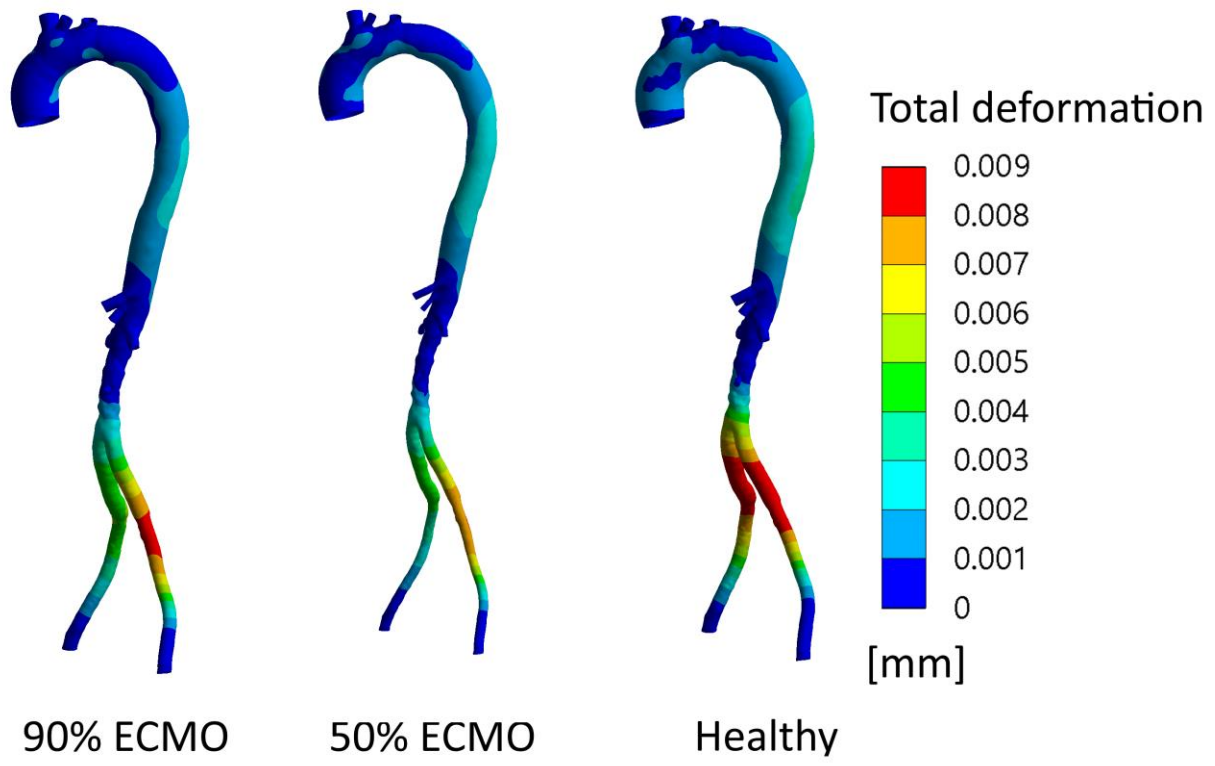
Author acc



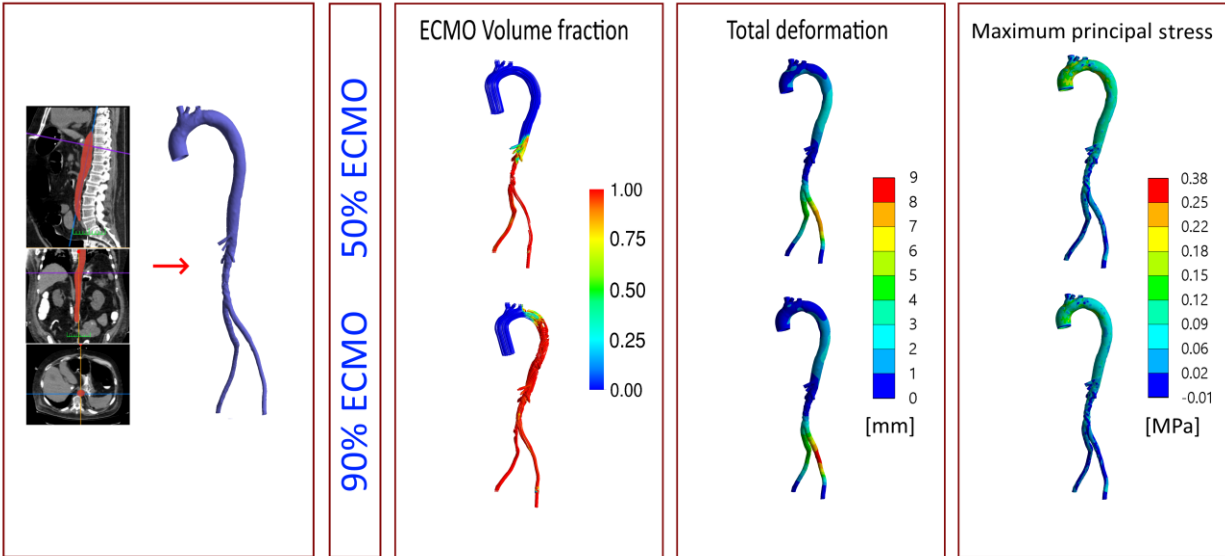
Author accepted manuscript



Author accepted manuscript



Author accepted



Author accepted manuscript